Structures of Cytochrome b_5 Mutated at the Charged Surface-Residues and Their Interactions with Cytochrome c †

WU, Jian[a](邬键) WANG, Yun-Hua[b](王韵华) GAN, Jian-Hua[a](甘建华)
WANG, Wen-Hu[b](王文虎) SUN, Bing-Yun[b](孙炳耘) HUANG, Zhong-Xian*,[b](黄仲贤)
XIA, Zong-Xiang*,[a](夏宗芗)

[a] *State Key Laboratory of Bioorganic and Natural Products Chemistry, Shanghai Institute of Organic Chemistry, Chinese Academy of Sciences, Shanghai 200032, China*

[b] *Chemical Biology Laboratory, Department of Chemistry, Fudan University, Shanghai 200433, China*

Glu44, Glu48, Glu56 and Asp60 are the negatively charged residues located at the molecular surface of cytochrome b_5. Two mutants of cytochrome b_5 were prepared, in which two or all of these four residues were mutated to alanines. The mutations give rise to slightly positive shifts of the redox potentials of cytochrome b_5 and obvious decrease of the cytochrome b_5-cytochrome c binding constants and electron transfer rates. The crystal structures of the two mutants were determined at 0.18 nm resolution, showing no alteration in overall structures and exhibiting slight changes in the local conformations around the mutation sites as compared with the wild-type protein. Based on the crystal structure of the quadruple-site mutant, a model for the binding of this mutant with cytochrome c is proposed, which involves the salt bridges from Glu37, Glu38 and heme propionate of cytochrome b_5 to three lysines of cytochrome c and can well account for the properties and behaviors of this mutant.

Keywords cytochrome b_5, mutant, crystal structure, interprotein interaction, electron transfer

Introduction

Microsomal cytochrome b_5 (Cyt b_5) is a member of cytochrome b_5 family, and it serves as an electron carrier in a series of electron-transfer processes in biological systems.[1-3] Cyt b_5 is a membrane protein with $M_r \sim 16$ kDa, consisting of two domains, one hydrophobic domain which anchors the protein to the membrane and one hydrophilic domain which contains heme group and is responsible for the biological activities.[4] The proteolysis of bovine liver microsomal Cyt b_5 by lipase and trypsin produces the soluble N-terminal fragments consisting of 93 residues (Ser1—Ser93) and 84 residues (Ala3—Lys86) respectively.[5] The recombinant trypsin-solubilized fragment of bovine liver microsomal Cyt b_5, referred to as Cyt Tb_5, was obtained in our laboratory, which contains 82 residues (Ala3—Arg84) and possesses the activity of Cyt b_5.[6]

Electron transfer is one of the basic chemical reactions in biological systems. The process of electron transport can be regarded as two separate steps, highly specific binding interactions between the redox proteins and the actual electron transfer reaction within the bound protein complex.[7]

Cyt b_5 and cytochrome c (Cyt c), as electron transfer proteins, widely exist in nature. The X-ray analyses of Cyt c and the lipid- or trypsin-solubilized fragments of Cyt b_5 provided the detailed information about the three-dimensional structures of the two proteins.[6,8-12] Cyt b_5-Cyt c is an attractive system for investigating the interprotein interactions and the electron transfer between the two proteins.

Cyt b_5 is an acidic protein with net charge -9, and

* E-mail: xiazx@pub.sioc.ac.cn; Tel.: 86-21-64163300; Fax: 86-21-64166128
Received May 1, 2002; revised and accepted June 25, 2002.
Project supported by the National Natural Science Foundation of China (Nos. 39970159, 29731030 and 39990600).
† Dedicated to Professor HUANG Yao-Zeng on the occasion of his 90th birthday.

Cyt *c* is a basic protein with net charge +7 at pH 7,[13] which suggests that the electrostatic interactions might be very important for the formation of the complex between the two proteins. The NMR studies indicate the existence of a 1:1 complex in solution between the two cytochrome proteins.[14] However, so far the X-ray or NMR structure of the Cyt b_5-Cyt *c* complex is unavailable. Salemme established the first Cyt b_5-Cyt *c* complex model by optimizing the intermolecular complementary charge and steric interactions using least-square fitting process,[15] and the model was then extended using molecular dynamics simulation method.[16] In this model there are four principal complementary charge interactions from Glu44, Glu48, Asp60 and the most exposed heme propionate of Cyt b_5 to Lys27, Lys13, Lys72 and Lys79 of Cyt *c*, respectively. The Brownian dynamics simulation modeling was carried out by Northrup *et al.*, and the results reveal that the first predominant complex model involves the following Cyt b_5-Cyt *c* interactions: Glu48-Arg13, Glu56-Lys87, Asp60-Lys86 and heme propionate-Tml72 (Tml72 denotes trimethyl Lys72), and the second prodominent one is consistent with the Salemme's model.[17]

Meyer *et al.*[18] reported the laser flash photolysis results, emphasizing the flexibility of electron transfer between Cyt b_5 and Cyt *c* and the existence of a variety of orientations within the protein-protein complex. Burch *et al.*[19] demonstrated by NMR that at least 6 lysyl residues of Cyt *c* were involved in the Cyt *c*-Cyt b_5 binding, and the two cytochromes form two or more structurally similar 1:1 complexes in the solution. Site-directed mutagenesis was used to examine the effects of the mutation of the charged surface-residues of Cyt b_5 or Cyt *c* on the protein-protein interactions and the electron transfer, such as the mutation from Glu43, Glu44, Glu48, Glu56 and Asp60 to the corresponding amide analogues.[20,21]

The two known binding models proposed by Salemme and Northrup[15-17] indicate that a total of 4 negatively charged surface residues, Glu44, Glu48, Glu56 and Asp60, of Cyt b_5 are involved in the electrostatic interactions for binding to Cyt *c*. We prepared a variety of mutants of Cyt *Tb*$_5$, mutated at these key residues, such as E44A, E56A and E44/56A, and the influences of the mutations on the interactions of Cyt b_5 with Cyt *c* and the electron transfer were previously reported.[22,23]

In order to further elucidate the molecular recognition and the mechanism of electron transfer between Cyt b_5 and Cyt *c*, we have prepared a quadruple-site mutant of Cyt *Tb*$_5$, E44/48/56A/D60A, with Glu44, Glu48, Glu56 and Asp60 all mutated to alanine,[24] which is referred to as Mut4. The solution structures of the mutants E44A, E56A, E44/56A and Mut4 were determined by NMR spectroscopy.[22,24] Since the solution structure of the wild-type Cyt *Tb*$_5$ is unavailable at present, no solution structure comparison was carried out between the mutants and the wild-type protein.

In this paper we present the crystal structures of Mut4 and E44/56A mutants, and compare them with the structure of wild-type Cyt *Tb*$_5$.[6] The redox potential variation of the two mutants and the electron transfer kinetics as a function of temperature and ionic strength are also reported in this paper. Based on the crystal structure of Mut4, molecular modeling method was used to investigate the docking geometry and the interactions of Mut4 with Cyt *c*, and a new binding model is proposed.

Experimental

Materials

Double-distilled water and analytic grade chemicals were used in the preparation of all the solutions. Methylviologen and proflavine hemisulfate were purchased from Tokyo Chemical Industry Co. Ltd.

Protein preparations

The pUC19 plasmid containing the synthesized gene encoding the Cyt *Tb*$_5$ (82 residues in length) was a kind gift from Professor Mauk.[25] Site-directed mutagenesis of the gene was described previously.[26] Mutant genes were identified by sequencing the single-stranded DNA and double-stranded DNA.[27] The expression of genes and the purification of proteins were described previously.[22] Horse heart Cyt *c* (type VI) was purchased from Sigma and further purified.[28] Protein concentrations were determined spectrophotometrically [$\varepsilon_{412.5}$ = 117000 $cm^{-1} \cdot (mol/L)^{-1}$ and $\varepsilon_{409.5}$ = 106100 $cm^{-1} \cdot (mol/L)^{-1}$] for ferricytochr-ome b_5[29] and ferricytochrome *c*,[30] respectively.

Crystallization and data collection

Crystals of the E44/56A and Mut4 mutants were grown in hanging drops by vapor diffusion method. The

reservoir solution consisted of 2.7—2.8 mol/L phosphate buffer (pH 8.0) for the E44/56A mutant, and of 3.1—3.2 mol/L phosphate buffer (pH 7.5) for Mut4. Equal amounts of the reservoir solution and the protein solution (20 mg/mL) were mixed into a 10 μL drop and the vapor diffusion was carried out at 20 ℃ for two weeks. The diffraction-quality crystals were obtained with a typical dimensions of 0.4 mm × 0.4 mm × 0.3 mm. The crystallizing conditions are similar to those of the wild-type Cyt Tb_5[6] and other mutants of Cyt Tb_5.[31]

Diffraction data were collected up to 0.18 nm resolution on a MarResearch Imaging Plate-300 Detector System (with an X-ray generator operating at 2 kW) using two and one crystal for each of E44/56A and Mut4 mutants, respectively. The images were processed using the program DENZO, and the data were scaled and merged using the program SCALEPACK,[32] giving R_{sym} of 4.5% and 7.2%, and the data completeness of 91.6% and 92.1% for the E44/56A and Mut4 mutants, respectively. The data collection statistics are presented in Table 1.

Crystal structure determination and refinement

The structure of the E44/56A mutant was determined using the difference Fourier method based on the crystal structure of F35Y refined at 0.18 nm resolution (unpublished results).

The determination of the initial structure of Mut4 was carried out using the molecular replacement method by applying the program Amore[33] of the CCP4 Suite.[34] The crystal structure of the wild-type Cyt Tb_5 at 0.19 nm resolution[6] was used as the search model, in which all the water molecules were omitted and the four mutated residues were replaced by alanine. The diffraction data in the resolution range of 1—0.4 nm were used for the calculation of rotation function and translation function as well as rigid body refinement. The initial structure model of Mut4 was obtained by applying the molecular replacement solution to the search model.

The programs X-PLOR[35] and CNS[36] were successively used for the crystallographic refinement of these two mutant structures. All the data up to 0.18 nm were used for structural refinement in the CNS stage. 10% of the data were randomly excluded from the refinement and used as the test data set to monitor R_{free}.[37] The model fitting was carried out with the graphics software TURBO-FRODO[38,39] on a Silicon Graphics Indigo 2 workstation.

The rigid body refinement was applied to the initial models of the E44/56A and Mut4 mutants, followed by a number of rounds of positional refinement and temperature-factor refinement. The resolution was gradually extended to 0.18 nm during the refinement. The $(2F_o - F_c)$ and $(F_o - F_c)$ electron density maps were regularly calculated for the model rebuilding. During the refinement, the solvent molecules were gradually included in the model when the resolution was extended up to 0.22 nm. Only those solvent molecules with temperature factors lower than 0.5 nm^2 and with reasonable hydrogen-bonding environment were included in the final model. In the CNS refinement stage the simulated annealing refinement[40] was carried out, starting from 2500 K with a cooling rate of 25 K per cycle, followed by the individual temperature-factor refinement, giving the final structural models of the two mutants.

Spectrophotometric study

The binding constants were determined by difference spectrophotometry on a HP8452A diode array spectrophotometer at (25 ± 0.2) ℃ according to the reported procedure.[22,41] Protein solutions were prepared by dissolving the lyophilized proteins in 1 mmol/L sodium phosphate buffer (pH = 7.0).

Spectroelectrochemical measurements

Spectroelectrochemical measurements were performed with a Hewlett-Packard 8452A diode array spectrophotometer at room temperature.[42] Spectra of fully reduced protein and fully oxidized protein were recorded at − 350 and + 120 mV (vs. SHE), respectively. The wild-type and the mutants of Cyt Tb_5 were dissolved in phosphate buffer, pH 7.0, I = 0.1 mol/L, containing 0.01 mmol /L $Ru(NH_3)_6Cl_3$ as a mediator at a protein concentration of 0.1 mmol/L.

Stopped-flow kinetics

Rate constants of electron transfer between ferrocytochrome b_5 and ferricytochrome c were measured by stopped-flow spectrophotometer in the described procedure.[22] The empirical dead time is less than 1 ms for the SF-61DX2 Double-Mixing Stopped-Flow spectrophotometer (1 cm observation path length) interfaced to a

Dell Dimension XPS M233s computer (Hi-Tech Scientific Company, UK). The temperature was maintained with a NESLAB RTE-5B circulating bath instrument, and the measurement accuracy was within ±0.2 ℃.

The kinetics of the inter-protein electron transfer was examined under the pseudo-first-order condition with the concentrations of Cyt b_5 and Cyt *c* at 3—5 μmol/L and 30 μmol/L respectively. Reduction of Cyt b_5 was completed by photo-reduction of a solution containing methylviologen/proflavin hemisulfate. Oxidation of Cyt b_5 by Cyt *c* was monitored at 428 nm where the total absorbance and the change in absorbance of Cyt *c* are small. At least ten absorbance changes obtained were averaged and fitted to a first-order rate expression to generate the electron transfer rate (appended on the KinetAsyst Software).

Molecular modeling

Molecular modeling of the interactions between Mut4 and Cyt *c* was carried out using the program CNS.[36]

The coordinates of the horse heart Cyt *c* were taken from the high resolution crystal structures,[11] and those of Mut4 from the crystal structure described in this paper. No water molecule was included in the models.

The Mut4 model was fixed, and the model of Cyt *c* was docked to the proximity of Mut4 by using the graphics software TURBO-FRODO, so that the positively-charged surface region of Cyt *c* could make contacts with the negatively-charged region of Mut4. A set of starting models were established, by altering the Cyt *c* orientation and position. The side chains of some residues located in the interface of the complex model were manually adjusted using TURBO-FRODO to avoid unreasonably close contacts with each other and to form as many salt bridges as possible.

For each of the starting model the energy was minimized for 200 cycles. Then the Cartesian molecular dynamics simulation was carried out, with the integration time of 0.005 ps, and 1000 steps were executed at 298 K, which was followed by another 200 cycles of energy minimization to generate a series of models of the Mut4-Cyt *c* complex. The final model was selected from a set of the generated models with the criteria of the minimum total energy and the most reasonable intermolecular interactions.

Throughout the energy minimization and molecular dynamics modeling procedure, no restraint was imposed except that the coordination geometry of the iron atoms were restrained, based on the crystal structures of Cyt Tb_5 and Cyt *c*, as follows: the coordination distances from iron to the nitrogen atoms NE2 of the axial ligands His39, His63 of Cyt b_5 and to NE2 of His18 of Cyt *c* were restrained to 0.205 nm, and that from iron to the sulfur atom of Met80 of Cyt *c* was restrained to 0.235 nm; the angle NE2 (His39)-iron-NE2 (His63) in Cyt b_5 was restrained to 180°.

Results

Crystal structures of the E44/56A *and* Mut4 *mutants*

The E44/56A mutant crystals belong to the monoclinic space group *C*2 with unit cell parameters of a = 7.069 nm, b = 4.049 nm, c = 3.920 nm and β = 111.43°, which are the same as those of the wild-type Cyt Tb_5. However, Mut4 crystallizes in the orthorhombic space group $P2_12_12_1$ with a = 4.093 nm, b = 4.088 nm and c = 5.295 nm. The crystal data are shown in Table 1.

The molecular replacement[43] solution of Mut4 is as follows: α = 86.32°, β = 48.40°, γ = 130.73°; T_x = 0.3038, T_y = 0.1396, T_z = 0.2374. The refinement statistics are also shown in Table 1. The R factor and R_{free} of the final model of the E44/56A mutant at 0.18 nm resolution are 19.3% and 23.2%, respectively, and those of Mut4 at 0.18 nm resolution are 19.4% and 23.8%, respectively. The r.m.s. (Root-mean-square) deviations from the ideal bond lengths and bond angles are 0.0010 nm and 1.22° for the E44/56A mutant structure, respectively, and 0.0009 nm and 1.18° for the Mut4 structure, respectively. The refinement statistics are summarized in Table 1.

The Ramachandran plots[44] of the models of the two mutants show that all the non-glycine residues are located within the acceptable regions, with 91.7% (E44/56A) and 93.1 % (Mut4) in the most favored regions respectively, validated by using the program PROCHECK.[45] The Luzzati plots[46] of the E44/56A and Mut4 mutants show that the estimated mean errors of the atomic coordinates are approximately 0.022 nm and 0.023 nm, respectively.

The overall structures of the E44/56A and Mut 4

Table 1 Data collection and refinement statistics

	E44/56A	Mut4
Space group	$C2$	$P2_12_12_1$
a (nm)	7.069	4.093
b (nm)	4.049	4.088
c (nm)	3.920	5.295
γ (°)	111.43	
Number of molecules per asymmetric unit	1	1
V_m(nm^3/Da)	0.00262	0.00225
Highest resolution (nm)	0.18	0.18
Number of unique reflections	8874	8012
R_{sym}(%)[a]	4.5 (22.8)[d]	7.2 (35.2)[d]
Data completeness (%)	91.6 (59.1)[d,e]	92.1 (75.5)[d]
$< I/3\sigma(I) >$[b]	18.2 (4.8)[d]	24.3 (6.9)[d]
No. of amino acid residues	82	82
No. of prosthetic group	1	1
No. of solvent molecules	91	89
R-factor (%)	19.3	19.4
Free R-factor (%)	23.2	23.8
r. m. s. d. Bond lengths (nm)[c]	0.0010	0.0009
r. m. s. d. Bond angles (°)[c]	1.22	1.18
Mean temperature factors		
Main chain (nm^2)	0.205	0.205
Side chain (nm^2)	0.247	0.225
Heme (nm^2)	0.237	0.180
Solvent (nm^2)	0.423	0.394

[a] R_{sym} = Sum[ABS($I - < I >$)]/Sum(I); [b] Mean signal-to-noise ratio; [c] Root-mean-square deviation; [d] The numbers in the parentheses correspond to the data in the highest resolution shell (0.180—0.184 nm). [e] The data completeness in the resolution shell (0.184—0.189 nm) is 74.5%.

mutants are similar to that of the wild-type Cyt Tb_5.[6] Fig. 1a shows the Cα backbone of Mut4, superimposed with that of the wild-type Cyt Tb_5. The r.m.s. deviations of all the Cα atoms are 0.008 nm between E44/56A and the wild-type Cyt Tb_5, and 0.029 nm between Mut4 and the wild-type Cyt Tb_5. The secondary structures are the same in the three molecules. However, the significant difference in the conformation of the molecular surface segment Asn16-Ser20 can be observed between Mut4 and either of the other two structures when the three structures are superimposed (Fig. 1a shows the difference between Mut4 and the wild-type Cyt Tb_5) although each of them contains a β-turn. Furthermore, the temperature factors of this segment are higher in Mut4 than those in Cyt Tb_5 and E44/56A.

Glu44, Glu48, Glu56 and Asp60 are located at the molecular surface of Helix III and Helix IV that are the components of the heme pocket wall of Cyt b_5,[6,8-10] and their side chains extend into the solvent, as shown in Fig. 1b. The mutations from two or four of these hydrophilic residues to the small hydrophobic alanine residues lead to slight changes in the local conformation

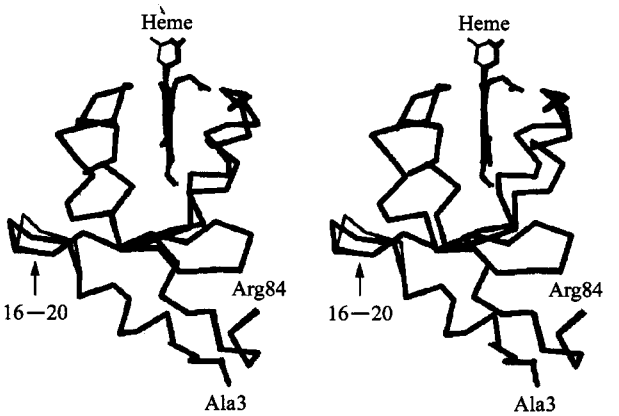

Fig. 1a Cα backbones and the hemes of the Mut4 mutant superimposed with the wild-type Cyt Tb_5. Wild-type Cyt Tb_5 is shown in thick lines, and Mut4 in thin lines. Ala3, Arg84 and the segment Asn16—Ser20 are indicated. This diagram was prepared using the molecular graphics program SETOR.[47]

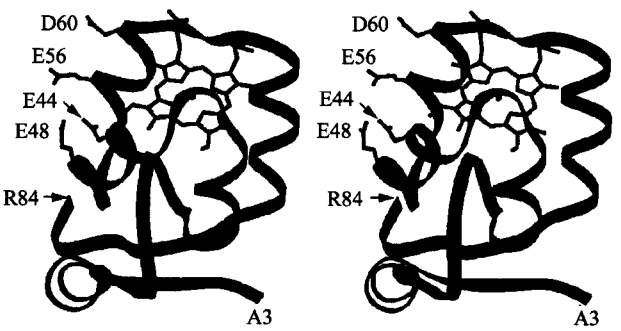

Fig. 1b The ribbon diagram of the wild-type Cyt Tb_5. The sidechains of Glu44, Glu48, Glu56 and Asp60 are shown. This diagram was prepared using the molecular graphics program SETOR.

around the mutation sites. Cα and Cβ atoms of Glu44 shift by approximately 0.03 nm and 0.04 nm respectively, and the segment around Glu44 (Glu43—Arg47) also shows a slight shift. The shifts of Cα and Cβ atoms of Glu48, Glu56 and Asp60 are very small, ranging from 0.009 nm to 0.018 nm.

The positions and the orientations of the heme in E44/56A and Mut4 are similar to those in the wild-type Cyt *Tb*$_5$. One of the two propionates forms two hydrogen bonds to the main- and side-chain atoms of Ser64, exhibiting the conserved conformation in the three structures. The other propionate extends into the solvent, and its conformation is very different in Mut4 from those in Cyt *Tb*$_5$ and the E44/56A mutant, as shown in Fig. 1a. The latter heme propionate does not interact with any protein atoms of the symmetry-related molecules in Cyt *Tb*$_5$ or the E44/56A mutant structures. However, in the Mut4 structure, this heme propionate is involved in an intermolecular interaction network by forming one hydrogen bond to a solvent molecule and two hydrogen bonds to the guanidinium group of Arg47 of a symmetry-related molecule. Two solvent molecules near the heme make bridges between the molecule at x, y, z and its symmetry-related molecule at $x + 1/2$, $-y - 1/2$, $-z$. These hydrogen bonding interactions make the conformation of this propionate very different from those in the wild-type Cyt *Tb*$_5$ and E44/56A mutant structures.

Redox potential

The redox potentials of the E44/56A and Mut4 variants are 7.5 mV and 15 mV, respectively, which are only slightly higher than those of the wild-type Cyt *Tb*$_5$ (4.5 mV) and its single-site mutants E44A (6.0 mV) and E56A (6.3 mV).[22]

Binding between Cyt b_5 *and* Cyt *c*

As reported by Mauk *et al.*,[41] the absorption change at γ-band in its electronic difference spectrum is considered to be an indication of the formation of Cyt b_5-Cyt *c* complex. The binding constant between the E44/56A mutant and Cyt *c* was determined using this method, showing that its association constant [$(1.14 \pm 0.05) \times 10^6$ $(mol/L)^{-1}$] was lower than those between Cyt *c* and the wild-type Cyt *Tb*$_5$, E44A or E56A [$(4.70 \pm 0.10) \times 10^6$ $(mol/L)^{-1}$, $(1.88 \pm 0.03) \times 10^6$ $(mol/L)^{-1}$, $(2.70 \pm 0.13) \times 10^6$ $(mol/L)^{-1}$, respectively], as previously reported.[22]

The binding of Mut4 with Cyt *c* was proved by NMR studies with the binding constant of 5.1×10^3 $(mol/L)^{-1}$, which is obviously lower than 2.2×10^4 $(mol/L)^{-1}$, the binding constant determined by the same method for the wild-type protein.[24]

Electron transfer between Cyt b_5 *and* Cyt *c*

Figs. 2 and 3 illustrate the dependence of electron transfer rate constant (k_{ET}) between Cyt *c* and the wild-type Cyt *Tb*$_5$ or its mutants on temperature and ionic strength, respectively. In Fig. 2, a weighted linear least-squares analysis of the electron transfer rates yields the thermodynamic parameters, activation enthalpy ($\Delta H^{\neq}$) and entropy ($\Delta S^{\neq}$) of the electron transfer reaction, which are listed in Table 2. The data of the activation enthalpy and entropy of the wild-type Cyt *Tb*$_5$ are in good agreement with those reported by Eltis *et al.*[13] The order of the electron transfer rate constants k_{ET} under the experimental conditions is as follows: wild-type Cyt *Tb*$_5$ > E44/56A > Mut4 (Table 2). The Oxidation of ferrocytochrome b_5 by ferricytochrome *c* strongly depends on the ionic strength, the k_{ET} dropping greatly with the increase of the ionic strength, as shown in Fig. 3.

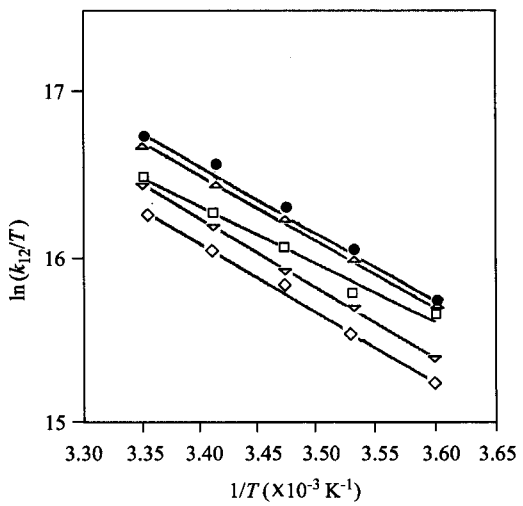

Fig. 2 Plots of the bimolecular rate constant of the reduction of ferricytochrome *c* by wild-type Cyt *Tb*$_5$ (●), E44A (□), E56A (△), E44/56A (▽), and Mut4 (◇) at different temperatures [I = 350 mmol/L, pH = 7.0 (phosphate)].

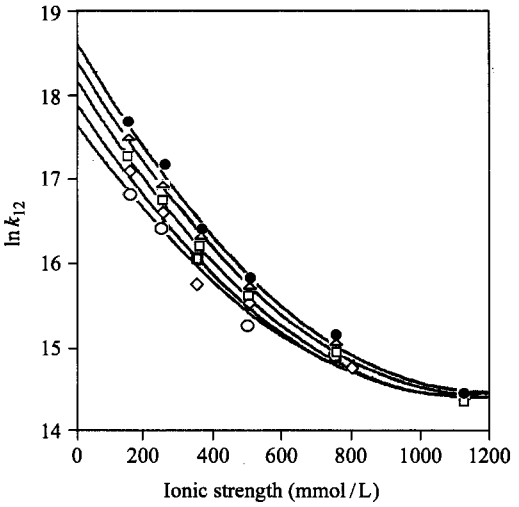

Fig. 3 Ionic strength dependence of the electron transfer rate constant ln k_{12} of the reduction of ferricytochrome *c* by wild-type Cyt Tb_5 (●), E44A (□), E56A (△), E44/56A (◇), and Mut4 (○) [T = (15 ± 0.2) ℃, pH = 7.0 (phosphate)]. The data points were empirically connected with a solid line. The error in the natural log of the second order rate constants is less than the size of the symbol.

Table 2 Thermodynamic and kinetic parameters for electron transfer between Cyt *c* and Cyt Tb_5 or its variants[a]

	Cyt Tb_5	E44/56A	Mut4
k_{12} [$\times 10^7$ $s^{-1}\cdot(mol/L)^{-1}$]	1.8	1.5	1.1
$\Delta S^{\neq}$ (eu)	−1.3	1.0	−1.0
$\Delta H^{\neq}$ (kJ/mol)	31.4	32.7	32.2

[a]The reactions were carried out under pH = 7.0 (phosphate), I = 350 mmol/L.

Interactions between Mut4 *and* Cyt *c*

A binding model for the interactions of Mut4 with Cyt *c* was generated by molecular modeling based on the crystal structure, which is shown in Fig. 4. It involves three inter-protein salt bridge interactions between the negatively charged residues of Mut4 and the positively charged residues of Cyt *c* at the molecular surface, *i.e.*, Glu37-Lys86, Glu38-Lys87 and heme propionate-Lys13. The salt bridge interactions are shown in Table 3. In addition to the salt-bridges, the main chain oxygen of Val61 of Mut4 forms a hydrogen bond to Gln12 side chain of Cyt *c*, also shown in Table 3.

The angle between the mean planes of Mut4 heme and Cyt *c* heme is about 20° in this binding model. Compared with Northrup's model, Cyt *c* in this binding model is rotated by approximately 180° along the axis running through the iron and the pyrrole nitrogen of ring D of Mut4 where the extended propionate protrudes to the solvent. The mean heme planes in the two binding models make an angle of approximately 50°. The iron-iron distance in this model is 1.84 nm, slightly longer than those reported for the wild-type Cyt b_5-Cyt *c* complex models (1.78 nm and 1.67 nm).[15, 17]

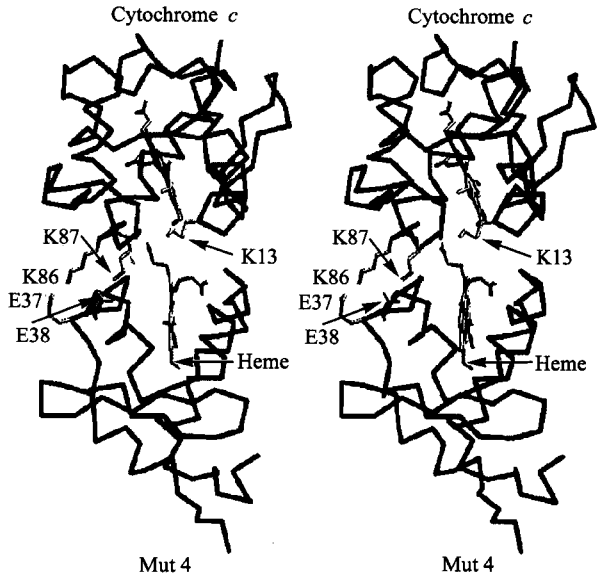

Fig. 4 The binding model of the Mut4-Cyt *c* system, generated by molecular modeling. The Cα backbones of both Mut4 and Cyt *c* are shown in black. The salt-bridged residues are shown in gray and labeled. This diagram was prepared using the program SETOR.

Table 3 The salt bridge and the hydrogen bond interactions in the Mut4-Cyt *c* system (atom 1 in Mut4, atom 2 in Cyt *c*)

Atom 1	Atom 2	Distance (nm)
E37 OE1	K86 NZ	0.26
E37 OE2	K86 NZ	0.27
E38 OE1	K87 NZ	0.27
E38 OE2	K87 NZ	0.26
Heme O1D	K13 NZ	0.27
V61 O	Q12 NE2	0.29

Discussion

Crystal packing

Glu44, Glu48, Glu56 and Asp60 are the negatively

charged residues located at the surface of Cyt Tb_5 molecule. Glu44 is close to a 2-fold axis of symmetry, and Glu44 of the two molecules related by the 2-fold axis are close to each other. The side chain of Glu56 of Cyt Tb_5 molecule at (x, y, z) is close to the main chain and side chain of Glu69 of the molecule at $(-x+1/2, y-1/2, -z)$. Each of the side chains of Glu44 and Glu56 in Cyt Tb_5 forms a hydrogen-bonding network which involves the symmetry-related molecules as well as two or three water molecules. Glu48 and Asp60 are far from other molecules.

In the E44/56A mutant, the crystal packing does not change due to the mutation although the hydrogen bonding networks involving Glu44 and Glu56 disappear. However, when all of the Glu44, Glu48, Glu56 and Asp60 are mutated to small hydrophobic alanine residues, the tight packing of the molecules can not maintain in space group $C2$, so that Mut4 crystallizes in a different space group $P2_12_12_1$. Three new hydrogen bonding networks involving the main-chain oxygen and nitrogen atoms of Ala44 and Ala48 are formed in Mut4 by introducing some new water molecules, while the water networks involving Glu44 and Glu56 in Cyt Tb_5 no longer exist in Mut4 structure.

Asn16—Ser20 is a flexible segment.[6] The conformational change of this segment was observed in Mut4 structure, which can be attributed to the different intermolecular interactions that result from different crystal packing. In the structures of Cyt Tb_5 and its E44/56A mutant, this segment forms five intermolecular hydrogen bonds with the protein atoms of a symmetry-related molecule. However, this segment is not involved in any intermolecular interactions in the Mut4 structure, which results in its conformation change and higher temperature factors.

Mut4-Cyt *c* interactions

For the mutant in which two negatively-charged surface residues were mutated to the non-polar alanines, the binding constant with Cyt *c* is lower than that of the wild-type Cyt Tb_5-Cyt *c* complex, as described above. NMR study demonstrated that although Mut4 does bind to Cyt *c*, as indicated by titrating Cyt *c* with Mut4 and recording the competitive paramagnetic difference spectra, the binding constant of Mut4-Cyt *c* determined by NMR is obviously lower than that of the wild-type Cyt Tb_5-Cyt *c* complex.

The electron transfer rate between the two proteins, which was measured by stopped flow technique, is also obviously lower for E44/56A-Cyt *c* and Mut4-Cyt *c* systems than that for the wild-type Cyt Tb_5-Cyt *c*, in the order of wild-type Cyt b_5 > E44/56A > Mut4.

The reduction potentials of the E44/56A and Mut4 mutants increase by +3.0 and +10.5 mV respectively, compared with that of the wild-type Cyt Tb_5. The small increase of the redox potentials resulting from the mutation is insufficient to give rise to the obvious decrease of the inter-protein binding and the electron transfer between the two proteins. Instead, this influence can be attributed to the difficulty in the molecular recognition resulting from the destruction of the salt bridges between the negatively charged residues of the Cyt b_5 mutants and the positively charged residues of Cyt *c* at the molecular interface. Each of the two known binding models indicates that the molecular recognition involves four salt bridges in the wild-type Cyt Tb_5-Cyt *c* complex. In the E44/56A mutant some of these salt bridges no longer exist, and in Mut4-Cyt *c* system more salt bridges are eliminated, resulting in the molecular recognition problem.

In either Salemme's or Northrup's model there is only one of the four salt bridges originally existing in the wild-type Cyt Tb_5-Cyt *c* complex remains in the Mut4-Cyt *c* system, *i.e.*, the one involving heme propionate, and the other salt bridges do not exist. However, the experimental results indicate that the inter-protein binding does exist and the electron transfer can still take place although its rate is slower, suggesting the flexibility of the docking geometry. While the two known models predominate over other binding models for the wild-type protein interactions, the population among the multi-binding models would alter when the charged surface residues are mutated to non-polar residues. In the case of Mut4 the known binding models with only one remaining salt bridge would be less favorable, and the binding model with three salt bridges, as shown in Fig. 4, would turn out to be the predominant one. Although the new binding model differs from Salemme's and Northrup's binding models, there are some common features in the three binding models, *i.e.*, the heme groups of the two proteins face each other, and the iron-iron distances are similar in the three models, which are required by the electron transfer. The new model well accounts for the inter-protein binding and the electron transfer in Mut4-Cyt *c* system. However, the reduction of the electrostatic interactions due to the muta-

tion results in the decrease of the binding constant and the slight increase of the iron-iron distance, consequently leading to decreasing the electron transfer rate.

On the other hand, the inter-protein interactions between Cyt b_5 and Cyt *c* include not only the electrostatic interactions but also the inter-protein hydrogen bonding and van der Waals interactions at the molecular interface region, for example, one hydrogen bond is observed at the Mut4-Cyt *c* interface.

Acknowledgements

We acknowledge Prof. A. G. Mauk of the University of British Columbia, Canada, for his kind gifts of Cyt b_5 gene. We are grateful to Prof. Li-Wen Niu, Prof. Mai-Kun Teng and Dr. Xue-Yong Zhu of the University of Science and Technology of China for their supports and help with the X-ray data collection.

Supplementary material

Atomic coordinates of E44/56A and Mut4 have been deposited in Protein Data Bank: 1M2I and 1M2M.

References

1 Hultquist, D. E.; Sannes, L. G.; Juckett, D. A. *Curr. Top. Cell. Regul.* **1984**, *24*, 278.
2 Sttrittmatter, P.; Spatz, L.; Corcoran, D.; Rogers, M. J.; Setlow, B.; Redline, R. *Proc. Natl. Acad. Sci. U. S. A.* **1974**, *71*, 4565.
3 Cohen, B.; Estabrook, R. W. *Arch. Biochem. Biophys.* **1971**, *143*, 54.
4 Spatz, L.; Sttrittmatter, P. *Proc. Natl. Acad. Sci. U. S. A* **1971**, *68*, 1042.
5 Mthews, F. S. *Prog. Biophys. Mol. Biol.* **1985**, *45*, 1.
6 Wu, J.; Gan, J.-H.; Xia, Z.-X.; Wang, Y.-H.; Wang, W.-H.; Xue, L.-L.; Xie, Y.; Huang, Z.-X. *Proteins: Struct., Funct. Genet.* **2000**, *40*, 249.
7 Stonehuerner, J.; Williams, J. B.; Millett, F. *Biochemistry* **1979**, *18*, 5422.
8 Mathews, F. S.; Levine, M.; Argos, P. *J. Mol. Biol.* **1972**, *64*, 449.
9 Mathews, F. S.; Argos, P.; Levine, M. *Cold Spring Harbersymp. Quant. Biol.* **1971**, *36*, 387.
10 Durley, R. C. E.; Mathews, F. S. *Acta Crystallogr., Sect. D: Biol. Crystallogr.* **1996**, *D52*, 65.
11 Dickerson, R. E.; Takano, T.; Eisenberg, D.; Kallai, O. B.; Samson, L.; Cooper, A.; Margoliash, E. *J. Biol. Chem.* **1971**, *246*, 1511.
12 Bushnell, G.; Louie, G. V.; Brayer, G. D. *J. Mol. Biol.* **1990**, *214*, 585.
13 Eltis, L.; Herbert, R. G.; Barker, P. D.; Mauk, A. G.; Northrup, S. H. *Biochemistry* **1991**, *30*, 3663.
14 Eley, G. S.; Moor, G. R. *Biochem. J.* **1983**, *215*, 11.
15 Salemme, F. R. *J. Mol. Biol.* **1976**, *102*, 563.
16 Wendoloski, J. J.; Matthews, J. B.; Weber, P. C.; Salemme, F. R. *Science* **1987**, *218*, 794.
17 Northrup, S. H.; Thomasson, K. A.; Miller, C. M.; Barker, P. D.; Eltis, L. D.; Guillemette, J. G.; Inglis, S. C.; Mauk, A. G. *Biochemistry* **1993**, *32*, 6613.
18 Meyer, T. E.; Rivera, M.; Walker, F. A.; Mauk, M. R.; Mauk, A. G.; Cusanovich, M. A.; Tollin, G. *Biochemistry* **1993**, *32*, 622.
19 Burch, A. M.; Rigby, S. E. J.; Funk, W. D.; Mac Gillivray, R. T. A.; Mauk, M. R.; Mauk, A. G.; Moore, G. R. *Science* **1990**, *247*, 831.
20 Rodgers, K. K.; Pochapsky, T. C.; Sliger, S. G. *Science* **1988**, *240*, 1657.
21 Rodgers, K. K.; Sliger, S. G. *J. Mol. Biol.* **1991**, *221*, 1453.
22 Sun, Y.-L.; Wang, Y.-H.; Yan, M.-M.; Sun, B.-Y.; Xie, Y.; Huang, Z.-X.; Jiang, S.-K.; Wu, H.-M. *J. Mol. Biol.* **1999**, *285*, 347.
23 Qian, W.; Sun, Y.-L.; Wang, Y.-H.; Zhuang, J.-H.; Xie, Y.; Huang, Z.-X. *Biochemistry* **1998**, *37*, 14137.
24 Wu, Y.-B.; Wang, Y.-H.; Qian, C.-M.; Lu, J.; Li, E.; Wang, W.-H.; Xie, Y.; Wang, J.-F.; Zhu, D.-X.; Huang, Z.-X.; Tang, W.-X. *Eur. J. Biochem.* **2001**, *268*, 1620.
25 Funk, W. D.; Lo, T. P.; Mauk, M. R.; Brayer, G. D.; MacGillivray, R. T. A.; Mauk, A. G. *Biochemistry* **1990**, *29*, 5500.
26 Yao, P.; Wang, Y.-H.; Xie, Y.; Huang, Z.-X. *J. Electroanal. Chem.* **1998**, *445*, 197.
27 Sanger, F.; Nicklen, S.; Coulson, A. R. *Proc. Natl. Acad. Sci. U. S. A.* **1977**, *74*, 5463.
28 Brautigan, D. L.; Miller, S. F.; Margoliash, E. *Methods Enzymol.* **1978**, *53*, 128.
29 Ozols, J.; Strittmatter, P. *J. Biol. Chem.* **1964**, *239*, 1018.
30 Margoliash, E.; Frohwirt, N. *Biochem. J.* **1959**, *71*, 570.
31 Xue, L.-L.; Wang, Y.-H.; Xie, Y.; Wang, W.-H.; Qian, W.; Huang, Z.-X.; Wu, J.; Xia, Z.-X. *Biochemistry* **1999**, *38*, 11961.
32 Otwinowski, Z.; Minor, W. *Methods Enzymol.* **1997**, *276*, 307.
33 Navaza, J. *Acta Crystallogr., Sect. A: Found. Crystallogr.* **1994**, *A50*, 157.
34 Collaborative Computational Project, Number 4. *Acta Crystal-*

logr., *Sect. D*: *Biol. Crystallogr.* **1994**, *D50*, 760.

35 Brunger, A. T. *X-PLOR*: *A System for X-Ray Crystallography and NMR* (*Version 3.1*), Yale University Press, New Haven, **1992**.

36 Brunger, A. T.; Adams, P. D.; Clore, G. M.; Delano, W. L.; Gros, P.; Gross-Kunstleve, R. W.; Jinag, J. S.; Kuszewski, J.; Nilges, N.; Pannu, N. S.; Read, R. J.; Rice, L. M.; Simonson, T.; Warren, G. L. *Acta Crystallogr.*, *Sect. D*: *Biol. Crystallogr.* **1998**, *D54*, 905.

37 Brunger, A. T. *Nature* **1992**, *335*, 472.

38 Jones, T. A. *Methods Enzymol.* **1985**, *115*, 157.

39 Roussel, A.; Cambillau, C. *TURBO-FRODO*, *Silicon Graphics Partner Geometry Dictionary*, Silicon Graphics Inc (eds), Mountain View, CA, **1991**, p. 86.

40 Brunger, A. T.; Kurijian, J.; Karplus, M. *Science* **1987**, *235*, 458.

41 Mauk, M. R.; Reid, L. S.; Mauk, A. G. *Biochemistry* **1982**, *21*, 1843.

42 Baymann, F.; Moss, D. A.; Mantele, W. *Anal. Biochem.* **1991**, *199*, 269.

43 Rossman, M. G. In *The Molecular Replacement Method*, Ed.: Rossman, M. G., Gordon & Breach, New York, **1972**, p. 4.

44 Ramachandran, G. N.; Sasasekharan, V. *Adv. Protein Chem.* **1968**, *28*, 283.

45 Laskowski, R. A.; MacArthur, M. W.; Moss, D. S.; Thornton, J. M. *J. Appl. Cryst.* **1993**, *26*, 283.

46 Luzzati, P. V. *Acta Crystallogr.* **1952**, *5*, 802.

47 Evans, S. V. *J. Mol. Graphics* **1993**, *11*, 134.

(E0205011 ZHAO, X. J.; FAN, Y. Y.)